New Investigations of the Guanine Trichloro Cuprate (II) Complex: (HGua)$_2$[Cu$_2$Cl$_6$]·2H$_2$O

Ivana Fabijanić[a], Dubravka Matković-Čalogović[b], Viktor Pilepić[a], Irena Ivanišević[a], Vlasta Mohaček-Grošev[c], and Krešimir Sanković*[d]

[a]University of Zagreb, Faculty of Pharmacy and Biochemistry, Department of Physical Chemistry, A. Kovačića 1, 10000 Zagreb, Croatia

[b]University of Zagreb, Faculty of Science, Department of Chemistry, Division of General and Inorganic Chemistry, Horvatovac 102A, 10000 Zagreb, Croatia

[c]Center of Excellence for Advanced Materials and Sensing Devices, Ruđer Bošković Institute, Bijenička c. 54, Zagreb, Croatia

[d]University of Zagreb, Faculty of Pharmacy and Biochemistry, Department of Biophysics, A. Kovačića 1, 10000 Zagreb, Croatia

*Correspondence e-mail: ksankovic@pharma.hr

Abstract

Crystals of (HGua)$_2$[Cu$_2$Cl$_6$]·2H$_2$O (HGua = protonated guanine) were prepared and analysed by spectroscopic (IR, Raman) and computational methods. A new single-crystal X-ray diffraction analysis was conducted to obtain data with lower standard uncertainties than those in the previously published structure. Raman and IR spectroscopy and quantum-mechanical analysis have given us new insight into the vibrational states of the (HGua)$_2$[Cu$_2$Cl$_6$]·2H$_2$O crystal. The vibrational spectra of the crystal were assigned by performing a normal coordinate analysis for a free dimer (HGua)$_2$[Cu$_2$Cl$_6$]·2H$_2$O with a centre of inversion as the only symmetry element. The stretching vibration observed at 279 cm^{-1} in the infrared spectrum corresponds to the N – Cu bond. The noncovalent interaction (NCI) plots and quantum theory of atoms in molecules (QTAIM) analysis of the electron density obtained form periodic DFT calculations gave us an insight into the interactions that exist within the crystal structure. Closed-shell ionic attractions, as well as weak and medium strength hydrogen bonds, prevailed in the crystal packing.

Introduction

The existence of electrical conductivity of the DNA molecule, i.e. the long-range charge migration along the DNA molecule, has been the subject of discussion of numerous publications for over half a century [1-3]. Test results are controversial; while some experiments show that DNA can carry electric current, other authors claim that DNA is not conductive. In our previous experiments, we examined the transfer of electrons / holes over great distances in single crystals of purine or pyrimidine bases using electron paramagnetic resonance (EPR) spectroscopy, and taking advantage of the spectroscopic properties of sulphur-centred radicals [4-11]. Single crystals of DNA bases were used as model systems of natural DNA. The stacking of the rings into a single crystal of the DNA base approximately corresponded to the base stacking in natural DNA [12-22], while water molecules and the present cations and anions represented the environment of a natural DNA molecule. The crystal structure of the complex "guanine·$CuCl_2$·HCl·H_2O" was published 45 years ago [23-24]. This paper presents new crystal data and a detailed crystal structure analysis of $(HGua)_2[Cu_2Cl_6]$·$2H_2O$ (HGua = protonated guanine), as well as a discussion of the related intermolecular contacts and packing. This crystal structure presents an interesting model system of natural DNA, because the environment of the guanine base consists of copper(II) and chlorine in the form of hexachlorodicuprate anions and of water molecules.

The spectroscopic data (IR and Raman) are presented and interpreted through a comparison with density functional theory (DFT)-calculated frequencies in order to investigate the bonding scheme within the molecule more deeply.

The intermolecular bonding networks between the guanine molecules, water molecules and ions in the crystal were explored with the aid of periodic DFT calculations. The wave function and electron density obtained for experimental atom coordinates in the crystal were analysed by noncovalent interaction (NCI) plots, pictorial representations of the intermolecular bonding interactions [25-27]. Furthermore, the nature of individual intermolecular interactions was examined in detail in terms of Bader's quantum theory of atoms in molecules (QTAIM) [28, 29].

Experimental

Crystal preparation

All of the chemicals used for synthesis were of analytical grade, purchased from Merck (guanine) and Kemika ($CuCl_2$, HCl) and used without further purification.

Complex $(HGua)_2[Cu_2Cl_6]\cdot2H_2O$ was prepared by dissolving 2.65 mmol (400 mg) of guanine (Merck) in a 20.0 ml water mixture of $CuCl_2\cdot2H_2O$ (3 mmol) and HCl (5 mmol). The resulting mixture was capped and then heated at 50ºC in a water bath for 1 h with continuous stirring and then left to slowly evaporate at about 300 K. The vessel containing the solution was covered with a watch glass to reduce evaporation. Approximately one month later, orange-brown crystals were obtained from a green solution (yield 63%) and remained stable months later while being exposed to the atmosphere. The crystals were of good quality for single-crystal X-ray diffraction.

Single crystal X-ray structure determination

Single crystal X-ray diffraction data were collected by ω-scans on an Oxford Diffraction Xcalibur 3 CCD diffractometer with graphite-monochromated MoK*α* radiation (λ = 0.71073 Å). A single crystal was glued onto a glass fiber and the data were collected at room temperature. Data reduction was performed using the CrysAlis software package [30]. The solution, refinement and analysis of the structure was done by the programs integrated within the WinGX system [31]. The structure was solved using direct methods within the SHELXS program [32]. The refinement procedure was performed by the full-matrix least-squares method based on F^2 against all reflections using SHELXL [30].

All non-hydrogen atoms were refined anisotropically. Hydrogen atoms were placed in calculated positions and refined using the riding model. The exceptions were the hydrogen atoms on the amino group and the water molecule, all of which were found in the difference Fourier map. The hydrogen atoms on the amino group were freely refined; however, those on the water molecule were not refined. Geometrical calculations were done using the PLATON program [33]. Drawings of the structure were prepared by the MERCURY program [34]. The crystallographic data are summarized in Table 1.

Table 1. Crystallographic data

empirical formula	$C_{10}H_{16}Cu_2Cl_6N_{10}O_4$
M_r	680.10
crystal system	monoclinic
space group	$C\,2/c$
unit cell parameters	
a (Å)	16.9887(9)
b (Å)	10.1895(4)
c (Å)	13.1822(4)
α (°)	90
β (°)	99.902(4)
γ (°)	90
V (Å^3)	2247.93(17)
Z	4
D_{calc} (g cm^{-3})	2.010
temperature (K)	295
wavelength (Å)	0.71073
μ (mm^{-1})	2.648
$F(000)$	1352
number of unique data	5531
number of data [$F_o \geq 4\sigma(F_o)$]	2971
number of parameters	153
R_1, wR_2 [$I \geq 2\sigma(I)$]	0.0330, 0.0746
R_1, wR_2 (all data)	0.0438, 0.0804
Goodness of fit on F^2, S	1.042
Min. and max. electron density (e Å^{-3})	-0.390, 0.428

Raman and IR spectroscopy

The Raman spectrum of the single crystal was obtained in the micro "single" mode of the T64000 HORIBA Jobin Yvon Raman spectrometer operating with grating set at 1800 grooves/mm. The green line (λ_o = 514.5 nm) of the argon ion laser served as an excitation source. Spectra were recorded in 10 repetitions with an accumulation time of 60 seconds. An objective with x50 magnification was used. Infrared spectra were obtained by milling the sample into powder with CsI and pressing it into a thin pellet. Spectra were recorded in transmission mode using an ABB Bomem MB102 Fourier transform infrared spectrometer with a DTGS detector and CsI optics averaging over 60 scans with a 4 cm^{-1} resolution.

Computational methods

In order to explore the IR and Raman spectroscopic data obtained for $(HGua)_2[Cu_2Cl_6]\cdot2H_2O$, the geometry optimization and frequency calculations of the dimer motif were performed in gas phase using the Gaussian03 [35] software package. The starting geometry for the calculation was taken from the experimentally determined crystal structure. The geometry optimization and frequency analysis were further performed with Perdew's electron correlation functional [36] and Perdew/Wang's PW91 exchange functional [37] (B3PW91) with 3-21/G basis set. Based on previous data for 1,1'-dimethyl-4,4'-bipyridinium hexachlorodicuprate [38] and piperazinium hexachlorodicuprate [39], the spin singlet ground state of the $(HGua)_2[Cu_2Cl_6]\cdot2H_2O$ system, separated by less than one meV from the upper triplet state, is expected. The calculated IR and Raman lines were compared with the experimentally obtained IR and Raman spectra lines for the crystal structure.

The initial atomic coordinates for periodic DFT calculations of the NCI plots and QTAIM descriptors for the $(HGua)_2[Cu_2Cl_6]\cdot2H_2O$ crystal cell were taken from the X-ray diffraction experiment. The calculations started with a geometry optimization of all of the hydrogen atoms within the entire crystal cell. The coordinates of all atoms heavier than hydrogen were fixed and the hydrogen atoms were fully geometry optimized under periodic conditions with a mixed Gaussian and plane wave CP2K software package [40, 41]. The periodic H atom geometry optimization in the crystal cell was performed with the PBE functional [42, 43], GTH pseudopotential [44, 45], optimized DZVP basis sets [46], 400 Ry cut-off for the plane wave grid and the Grimme D3 dispersion correction [47]. The single point calculation of the obtained H atom optimized geometry of the cell was performed with CP2K software using the

PBE functional, GTH-type pseudopotential, optimized TZVP-MOLOPT basis sets for H, N, C, O and Cl atoms and DZVP-MOLOPT-SR basis sets for Cu atoms [46], 1400 Ry cut-off for the plane wave grid and the Grimme D3 dispersion correction [47] in order to obtain the wave functions and electron density of the periodic cell. The pictorial representations of the NCI plots and Bader's QTAIM topological analysis from the obtained periodic electron density were calculated using the CRITIC2 [48] and VMD [49] software packages.

Results and discussion

Sundaralingam and Carrabine [24] reported crystals of two different forms and colours, yellow-brown single crystals and polycrystalline dark brown ones. In their preparation, they used a guanine:($CuCl_2 \cdot 2H_2O$) ratio of 1:4.3, whereas in our preparation that ratio was 1:1.1, which is why our experiment had only a small excess of copper(II) chloride. We obtained only one type of crystal, which was of orange–brown in colour and which proved to be the same as those previously described as yellow–brown in [24].

Crystal structure determination

The asymmetric unit encompassed one half of the dinuclear copper complex of guanine, $(HGua)_2[Cu_2Cl_6] \cdot 2H_2O$, with the two parts related by the inversion centre, Fig. 1. A study on guanine [50] found that the molecule was protonated at the nitrogen atom N9, whereas N3 and N7 were not protonated. In our structure, the guaninium cation was protonated at N3 and N7 and bonded to the copper atom through N9 at a distance of 1.9816(17) Å. The bond lengths from our experiment and angles are given in Table 2.

Furthermore, the present structure had lower standard uncertainties than those found in two other previously and independently published studies from different research groups [23, 24], and we have located hydrogen atoms on the water molecule's O2 atom.

Declercq *et al.* [23] described briefly the geometry of the copper coordination sphere and compared the interatomic distances and angles in the guaninium cation with guanine in other structures, whereas Sundaralingam and Carrabine [24] discussed in detail the crystal structure of $(HGua)_2[Cu_2Cl_6] \cdot 2H_2O$. They proposed that the first process is the protonation of all of the sites, followed by the deprotonation of N9, after which binding to the copper atom occurs.

The binding to the copper atom is sufficiently strong to compete with the proton for that site. They concluded that the electronic distortion of the guanine ring is mainly due to the protonation, while metal binding is of secondary importance. At the time of publication, the two groups could compare the molecular structures of the guaninium cation in the copper complex only with that of guanine monoprotonated at N7 [18], and with neutral guanine [50].
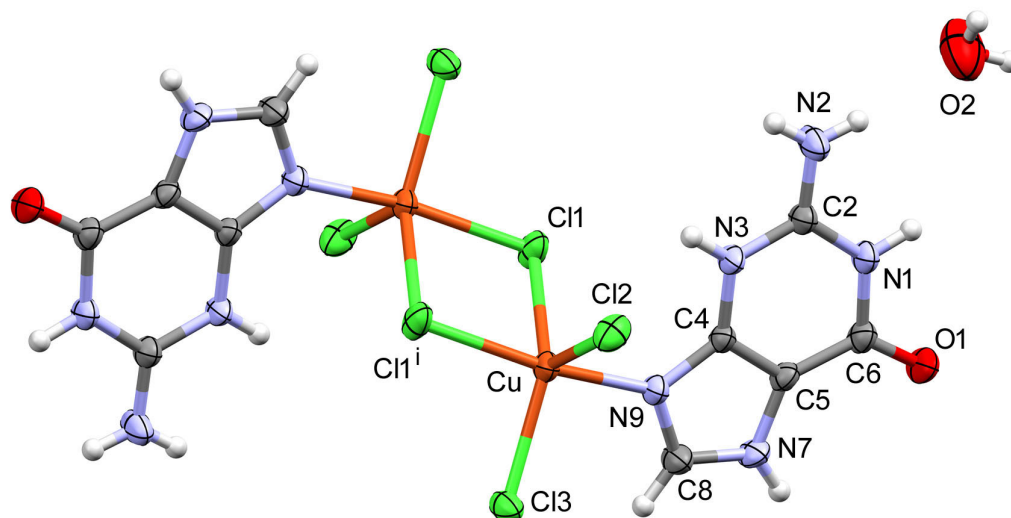
Fig. 1. Structure of (HGua)$_2$[Cu$_2$Cl$_6$]·2H$_2$O with an atom labelling scheme. The centrosymmetrically related water molecule is not shown. The thermal ellipsoids are at 50% probability level. Hydrogen atoms are drawn as spheres of arbitrary radii. The symmetry transformation used to generate equivalent atoms was: (i) –x+1/2, -y+1/2, -z.

This study enables the comparison of the guaninium ligand structure with the structure of guaninium dichloride we reported earlier [19], which also had all of its nitrogen atoms protonated. There is a significant difference in the angles involving N9 bonded to the Cu atom. The angle C4–N9–C8 is smaller in the present structure in comparison with that of guaninium dichloride, 104.83(18)º *vs.* 108.0(2)º, whereas the neighbouring angles are larger, N9–C4–C5, 110.4(2) *vs.* 107.6(2)º, and N9–C8–N7, 111.7(2)º *vs.* 109.3(2)º. This effect can be attributed to metal binding. Similar values were found in the guaninium complex with ruthenium(III) tetrachloride [51], and in the complex with platinum(II) trichloride [52]. Interestingly, the largest differences in the bond lengths of the present structure and guaninium dichloride involved the C2 atom within the six-membered ring, with the bond C2–N1 being longer with 1.365(3) Å and 1.347(3) Å, respectively, and C2–N3 being shorter

with 1.338(3) Å and 1.361(3) Å, respectively. This was influenced by much stronger hydrogen bonds in the structure of guaninium dichloride where the chloride atoms lie in plane with the guaninium cation.

The guaninium cation is bonded to the copper atom in a *trans*-position to the bridging Cl1[i] atom (Fig. 1). The Cu−Cl1[i] bond represents the shortest Cu−Cl distance in the dinuclear unit $[Cu_2Cl_6]^{2-}$ (Table 2). Until now, only four other crystal structures comprising a dinuclear unit $[Cu_2Cl_6]^{2-}$ with a Cu bonded additionally to a nitrogen atom from a ligand have been published. Of these, two had the N atom bonded *trans* to a bridging Cl atom [53, 54], being in the plane with two Cu atoms and two bridging Cl atoms, and with a trigonal-bipyramidal coordination of the Cu atom, as in our structure, which had the shortest Cu−N and Cu−Cl1[i] bonds. In the other two structures [55], the N atom from the ligand was bonded almost perpendicularly to the plane where two Cu and two bridging Cl atoms are located, and the coordination polyhedron around Cu was square-pyramidal.

All of the hydrogen atoms were involved in hydrogen bonds as presented in Fig. 2. Their lengths and angles are presented in Table 3. The hydrogen bonds interconnect the complex and water molecules into a 3D network, Fig. 3. Most of the hydrogen bonds are present in layers containing guaninium ligands and terminal chlorine atoms. Such a layer is separated from the neighbouring ones by bridging Cu_2Cl_2 units on one side, and a layer of water molecules on the other. N1−H1 and N7−H7 form hydrogen bonds to terminal Cl atoms, Cl2 and Cl3, from two different adjacent complex molecules. The amino group forms two hydrogen bonds, one to O3 of a neighbouring complex molecule and the other to O2 of the water molecule. N3−H3 is also hydrogen bonded to O3. The water molecule is a hydrogen bond donor to Cl2 within the layer, and weakly to Cl3 from the adjacent layer. Bridging Cl atoms are not involved in hydrogen bonding. Only the geometry of the hydrogen bonds that include the water molecule is significantly different from that reported by Sundaralingam and Carrabine [24].

Table 2. Bond distances (Å) and bond angles (º) in the crystal structure of $(HGua)_2[Cu_2Cl_6]\cdot 2H_2O$.

Bond distance		Angle	
Cu–N9	1.9816(17)	N9–Cu–Cl1[i]	168.91(6)
Cu–Cl1[i]	2.2881(6)	N9–Cu–Cl3	92.61(6)
Cu–Cl3	2.3300(7)	Cl1[i]–Cu–Cl3	94.20(2)
Cu–Cl2	2.3711(7)	N9–Cu–Cl2	90.98(6)
Cu–Cl1	2.4532(7)	Cl1[i]–Cu–Cl2	94.61(3)
Cl1–Cu[i]	2.2881(6)	Cl3–Cu–Cl2	111.76(3)
N1–C2	1.365(3)	N9–Cu–Cl1	86.83(6)
N1–C6	1.392(3)	Cl1[i]–Cu–Cl1	82.14(2)
C2–N2	1.303(3)	Cl3–Cu–Cl1	133.85(3)
N3–C2	1.338(3)	Cl2–Cu–Cl1	114.39(3)
N3–C4	1.371(3)	Cu[i]–Cl1–Cu	97.86(2)
O1–C6	1.237(3)	C8–N7–C5	107.48(19)
C5–C4	1.371(3)	N7–C5–C4	105.6(2)
C5–C6	1.413(3)	N7–C5–C6	132.9(2)
N7–C8	1.334(3)	C4–C5–C6	121.5(2)
N7–C5	1.365(3)	C2–N3–C4	119.23(17)
N9–C8	1.337(3)	C2–N1–C6	126.3(2)
N9–C4	1.357(3)	O1–C6–N1	120.4(2)
		O1–C6–C5	127.2(2)
		N1–C6–C5	112.39(18)
		N2–C2–N3	120.9(2)
		N2–C2–N1	120.4(2)
		N3–C2–N1	118.7(2)
		C8–N9–C4	104.83(18)
		C8–N9–Cu	126.68(17)
		C4–N9–Cu	128.41(15)
		N9–C4–N3	127.83(18)
		N9–C4–C5	110.4(2)
		N3–C4–C5	121.8(2)
		N7–C8–N9	111.7(2)

Symmetry transformation used to generate equivalent atoms: (i) -x+1/2, -y+1/2, -z

Fig. 2. Network of hydrogen bonding (blue dotted lines) within one layer that includes one half of three complex molecules, and two water molecules. The donor and acceptor atoms in the central molecule are labelled black, and those of the neighbouring molecules are labelled blue. For their symmetry code, see Table 3.
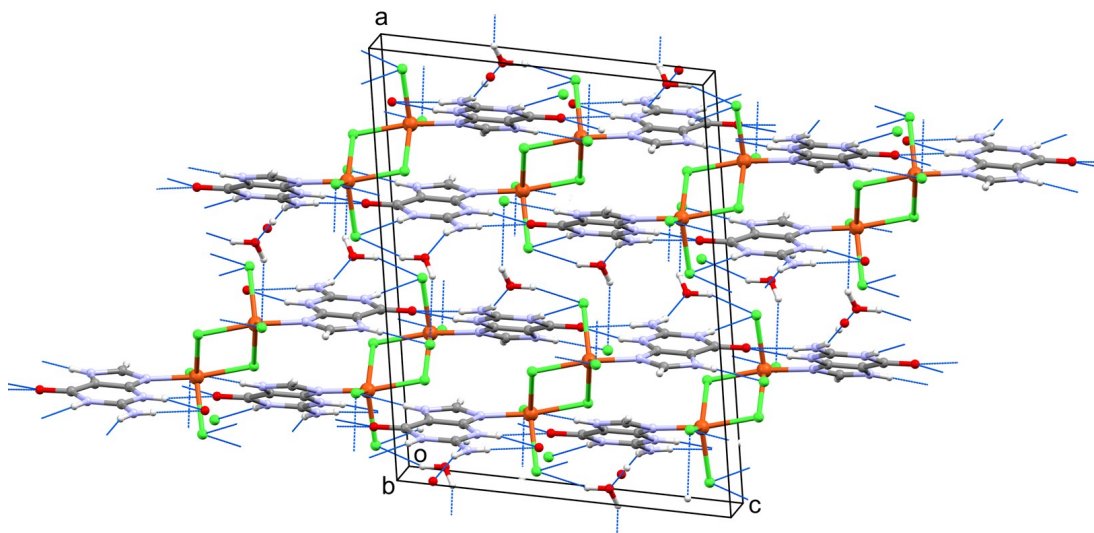
Fig. 3. Packing of (HGua)$_2$[Cu$_2$Cl$_6$] complex molecules and water molecules in the unit cell. The hydrogen bonds are shown as thin blue lines.

Table 3. Hydrogen bond geometry (Å, °).

	d(D–H)	d(H⋯A)	d(D⋯A)	∠(D–H⋯A)	Symmetry code
N1–H1⋯Cl2	0.86	2.28	3.117(2)	165	x,1-y,1/2+z
N2–H2A⋯O2	0.79(3)	2.08(3)	2.841(4)	161(3)	
N2–H2B⋯O1	0.77(4)	2.19(4)	2.895(3)	154(4)	x,1-y,-1/2+z
N3–H3⋯O1	0.86	2.13	2.885(3)	146	x,1-y,-1/2+z
N7–H7⋯Cl3	0.86	2.29	3.153(2)	178	x,-y,1/2+z
O2–H21⋯Cl3	0.89	2.68	3.421(3)	141	-1/2+x,1/2+y,z
O2–H22⋯Cl2	0.89	2.62	3.251(3)	129	1/2-x,1/2-y,-z
C8–H8⋯Cl1	0.93	2.61	3.353(3)	137	1/2-x,-1/2+y,1/2-z

IR and Raman spectra

The IR and Raman spectra of $(HGua)_2[Cu_2Cl_6]\cdot 2H_2O$ are presented in Fig. 4. Also, detailed assignations of the obtained IR and Raman bands and the data obtained from geometry optimization and frequency DFT calculations for the molecule unit in the gas phase are presented as supplementary data, Table S1. There are four formula units in the conventional unit cell altogether yielding 192 atoms. Consequently, the number of optical crystal phonons expected was large:

$$\Gamma_{vib} = 144\,A_g \oplus 144\,B_g \oplus 143\,A_u \oplus 142\,B_u$$

The Raman active modes belong to the A_g and B_g, while the infrared active modes belong to the A_u and B_u irreducible representations. The obtained Raman spectra, Fig. 4, and band positions and assignations in Table S1 can be compared with the Raman spectra of pure guanine previously assigned by Majoube et al. [56, 57], and by Giese and McNaughton [58]. The observed bands of polycrystalline pure guanine were compared with the calculated Raman shifts of normal modes of free guanine [57] and guanine heptahydrate [58]. As far as $(HGua)_2[Cu_2Cl_6]\cdot 2H_2O$ is concerned, it is evident that neither all of the 288 Raman modes nor all of the 285 infrared modes are observable in the crystal. The reason for that is the fact that Davydov's splitting from the vibrational modes of different molecular units, with slightly different vibrations due to molecular interactions, is not resolved. This splitting is less than the bandwidth of an observed band. Also, there is an overlap of different vibrational transitions of the dimer which prevents all of the bands from being resolved.

For $(HGua)_2[Cu_2Cl_6]\cdot 2H_2O$ in the gas phase with only a centre of inversion as a symmetry element, the following number of internal modes is expected:

$$69\,A_g \oplus 69\,A_u$$

Characteristic bands from pure guanine corresponding to C–N stretching vibrations were assigned to 1638 cm⁻¹, IR band, and 1604 cm⁻¹, Raman band [57], and to the 1551 cm⁻¹ Raman band [58]. The carbonyl-stretching vibrations observed in the Guanine Trichloro Cuprate (II) Complex were at 1704 cm⁻¹ in the Raman spectrum and at 1703 cm⁻¹ in the IR spectrum. C–N stretching vibrations lie below the water bending mode at 1635 cm⁻¹; they are

at 1596 and 1560 cm^{-1} in the Raman spectrum and at 1593 cm^{-1} and 1562 cm^{-1} in the IR spectrum. In our measurements, a strong Raman band at 1624 cm^{-1} was attributed to the C5=C4 stretching vibration. Several in plane N−H and C−H bending modes lie in the 1380-1500 cm^{-1} interval, below which they are mixed with N9−C8 stretching and N7−C5 stretching modes. Pyrimidine ring breathing mode at 1009 cm^{-1} is a very strong Raman band, observed often and not very sensitive to ring substitution. The binding of copper causes several important changes: the ν(Cu−Cl2) stretching vibration was calculated at 107 cm^{-1} and 105 cm^{-1} in the guanine dimer and occurred partially in a mixed A_g mode at 279 cm^{-1}, while the 195 cm^{-1} Raman band was attributed to the Cu−N9−C4 bending mode. Several notable copper related modes are the ν(Cu−N9) stretching mode predicted to lie at 279 cm^{-1} in the infrared spectrum, and ν(Cu−Cl2) Raman active stretching mode predicted at 105 cm^{-1}. While there is an infrared mode observed at 290 cm^{-1}, a low frequency Raman spectrum was not recorded due to a too low signal.

The theoretical value of the Cu−Cl stretching Raman vibration may be of particular interest in research related to superconductive materials with copper and chlorine as constituents [59]. The infrared spectrum displayed a very strong group of bands between 2680 cm^{-1} and 3570 cm^{-1}. The NH$_2$ asymmetric stretching modes have the highest frequency, below which the majority is assigned as ν(N–H) stretching vibrations. Besides, four ν(C–H) stretching bands are still unresolved. A very strong group of bands between 1500 and 1800 cm^{-1} comprises carbonyl stretching, water bending and NH in plane bending vibrations. For details see Table S1 in Supplementary Data.
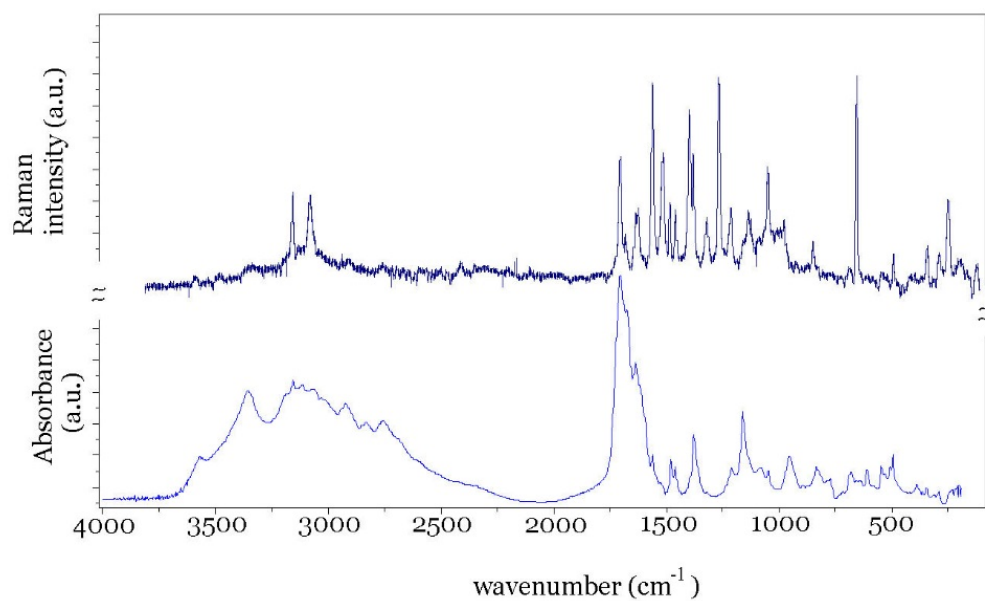
Fig. 4. IR and Raman spectra of the crystalline (HGua)$_2$[Cu$_2$Cl$_6$]·2H$_2$O.

Computational analysis

The intermolecular attractive interactions between HGua ligands, water molecules and Cu and Cl ions within the crystal cell are explored with NCI and QTAIM descriptors. The NCI descriptor, developed by Johnson *et al.* [25] and based on electron density and its derivative analysis, enables the visualization of domains in real space involved in either attractive or repulsive intermolecular interactions. NCI plots are obtained by plotting the sign(λ_2)$\rho(r)$ values with two cut-off values, ρ^+_{cut} and $\bar{\rho}_{cut}$, colour-mapped onto the reduced density gradient (RDG) isosurface, $s(r)$. The density cut-off values are used for setting the colour scale of the obtained domains, usually red-green-blue for ρ^+_{cut} (red) and $\bar{\rho}_{cut}$ (blue), interpreted as repulsive non-bonding, weak attractive and strong attractive interactions, respectively, between molecules in solids [25-27]. NCI plots have been successfully applied in research on hydrogen and halogen bonds, electrostatic, π-, lone pair and van der Waals interactions, molecular aggregations and crystal packing [26, 27].

The NCI plot obtained from the periodic cell electron density for a representative cluster unit in the crystal are shown in Fig. 5. The high-density domains represented as blue ellipsoids in bonds Cu–N9, Cu–Cl2, Cu–Cl3 and Cu–Cl1[i] suggest a strong attraction that can be attributed to ionic interactions. Also, the strong repulsion represented by the red ellipsoid in Cu···Cl1 contact, and also a very weak attraction represented with the green ellipsoid in Cl1[i]···Cl contact suggesting weak van der Waals interaction, were found between the ions. The attractive domains represented with green and blue ellipsoids, which can be attributed to hydrogen bonds between a single HGua ligand and the surroundings in the crystal cell, were also found and can be seen in Fig. 5. The nature of the intermolecular interactions in the structure of (HGua)$_2$[Cu$_2$Cl$_6$]·2H$_2$O are characterized by a topological analysis of the electron density within the Bader's QTAIM [28, 29]. Within the framework of QTAIM, the bond path (3,-1) critical point (BCP), the point on the bond path with minimal density value, properties are used to analyse and classify intermolecular interactions. The electron density, $\rho(r)$, and the magnitude and sign of the energy density, $H(r)$, on the BCP are related to bonding strength. The value of the Laplacian of the electron density, $\nabla^2\rho(r)$, on the BCP indicates a degree of density concentration or depletion and can be used to distinguish between shared-shell and closed-shell bonding interactions. The value of the Laplacian of the electron density is negative for shared-shell covalent bonding and positive for closed-shell bonding such as ionic, hydrogen-bond and van der Waals interactions. The potential energy density, $V(r)$, value at

BCP is correlated with the hydrogen-bond energy. The potential energy density and the kinetic energy density ratio, $|V(r)|/G(r)$, has a value larger than 2 for covalent bonds, between 1 and 2 for mixed character interactions and a value lower than 1 for ionic, hydrogen-bond and van der Waals interactions [29, 60, 61]. The representation of the selected bond path (3,-1) critical points (BCP 1-13) and their properties for interaction of a single unit with its surroundings in the crystal packing is presented in Fig. 6 and Table 4.

In general, the NCI plots resembled the obtained BCPs. For BCP 1 (N9–Cu), an electron density value, positive Laplacian and energy density values, negative potential energy density value and a potential energy density and kinetic energy density ratio lower than 1 was obtained, suggesting a very strong closed-shell ionic bonding interaction [29, 60, 61]. BCPs 2-5 associated with the Cu–Cl bonds, (Fig. 6 and Table 4), with large electron density values, positive Laplacian and energy density values, negative potential energy density values, and a potential energy density and kinetic energy density ratio lower than 1, suggest strong closed-shell ionic attractions somewhat weaker than Cu–N9 bonding. BCP 5 (Cu–Cl1) had slightly lower values of electron density, Laplacian and a potential energy density and kinetic energy density ratio than the corresponding values for BCP's 2-4 for other Cu–Cl interactions, suggesting weaker closed-shell ionic bonding, which is also reflected in the longer Cu–Cl1 bond distance of 2.4532(7) Å (Table 2) and a repulsive interaction domain observed in the NCI plot (Fig. 5). BCPs 6-13 are on bond paths that connect the attractors attributed to H atom and O or Cl atom and can be characterized as descriptors for hydrogen bonds in the crystal. Taking into account the positive Laplacian and energy density values and the potential energy density and kinetic energy density ratio values for BCP's 6-13 (Table 4) as well as the donor-acceptor distance (Table 3), the hydrogen bonds can be characterized as being of weak and medium strength with noncovalent and partially covalent closed-shell bonding interaction [61]. BCP 6 (Cl2···H1) and BCP 7 (Cl3···H7) had a large electron density, Laplacian values and potential energy density and a kinetic energy density ratio lower than 1, suggesting a medium strength hydrogen bond with noncovalent character. BCP 8 (Cl2···H22), the interaction of the Cl atom with the water molecule in the crystal, had a small electron density and Laplacian values, and a potential energy density and kinetic energy density ratio between 1 and 2, suggesting a weak hydrogen bond with partially covalent character. BCP 9 (O2···H2A), the interaction of the HGua ligand with the crystal water molecule, had a large electron density, Laplacian, and energy density values, and a potential energy density and kinetic energy density ratio lower than 1, suggesting a medium strength hydrogen bond of noncovalent character. For the bifurcated hydrogen bond with the over-coordinated O1

acceptor, contacts O1···H2B and O1···H3, and the corresponding BCP 10 and BCP 11 had moderate electron density, Laplacian and energy density values, a large potential energy density value and a potential energy density and kinetic energy density ratio about 2 and more, suggesting medium strength hydrogen bonds of partially covalent character. BCPs 12 and 13, the interactions of Cl1···H8 and Cl3···H21, respectively, with small electron density and Laplacian values, and a potential energy density and kinetic energy density ratio larger than 2 can be classified as weak hydrogen bonds with mixed character interactions. Beside these connections, weak van der Waals interactions were found between molecules and ions in the crystal as pockets around the Cl atoms, Fig. 5 and Fig. S2 in Supplementary Data. Taking into account the obtained QTAIM descriptors and NCI plots, the closed-shell ionic attractions and hydrogen bonds were predominant as the interactions in the crystal packing.

Table 4. The QTAIM descriptors of the selected bond path (3, -1) critical points (BCP) for intermolecular interactions in the $(HGua)_2[Cu_2Cl_6]\cdot 2H_2O$ crystal structure (Fig. 6). The electron density, $\rho(r)$, the Laplacian of the electron density, $\nabla^2\rho(r)$, the kinetic energy density, $G(r)$, the potential energy density, $V(r)$, the energy density, $H(r)$ and the ratio of the potential energy to the kinetic energy density, $|V(r)|/G(r)$ are presented in atomic units.

BCP		$\rho(r)$	$\nabla^2\rho(r)$	$G(r)$	$V(r)$	$H(r)$	$|V(r)|/G(r)$
1	Cu–N9	0.0874	0.2628	0.0494	-0.0332	0.0163	0.6721
2	Cu–Cl1[i]	0.0664	0.1514	0.0313	-0.0248	0.0065	0.7923
3	Cu–Cl2	0.0567	0.1470	0.0240	-0.0113	0.0127	0.4708
4	Cu–Cl3	0.0615	0.1569	0.0275	-0.0158	0.0117	0.5745
5	Cu–Cl1	0.0481	0.1241	0.0183	-0.0055	0.0128	0.3005
6	Cl2···H1	0.0327	0.0718	0.0096	-0.0012	0.0084	0.1250
7	Cl3···H7	0.0318	0.0691	0.0092	-0.0011	0.0081	0.1196
8	Cl2···H22	0.0184	0.0511	0.0037	0.0055	0.0091	1.4865
9	O2···H2A	0.0340	0.1015	0.0102	0.0049	0.0151	0.4804
10	O1···H2B	0.0222	0.0862	0.0050	0.0115	0.0165	2.3000
11	O1···H3	0.0225	0.0816	0.0052	0.0101	0.0152	1.9423
12	Cl1···H8	0.0144	0.0467	0.0025	0.0068	0.0092	2.7200
13	Cl3···H21	0.0131	0.0372	0.0021	0.0051	0.0072	2.4286
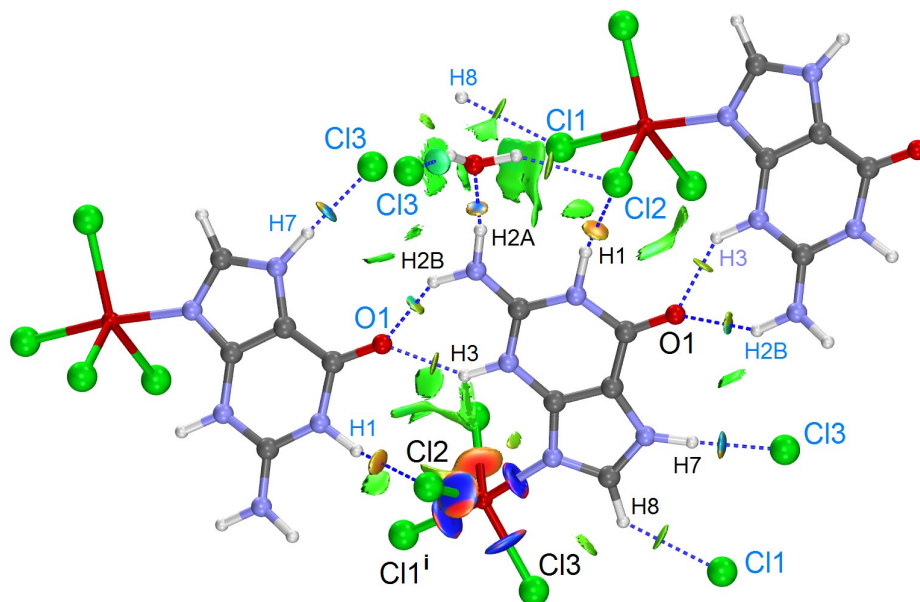
Fig. 5. The selected non-covalent interaction (NCI) domains in the (HGua)$_2$[Cu$_2$Cl$_6$]·2H$_2$O crystal. The reduced gradient isosurfaces at s = 0.4 a.u. are given in a red-green-blue colour scale according to the sign(λ_2)ρ values ranging from -0.05 to 0.05 a.u. indicating the repulsive non-bonding, weak attractive and strong attractive interactions, respectively.
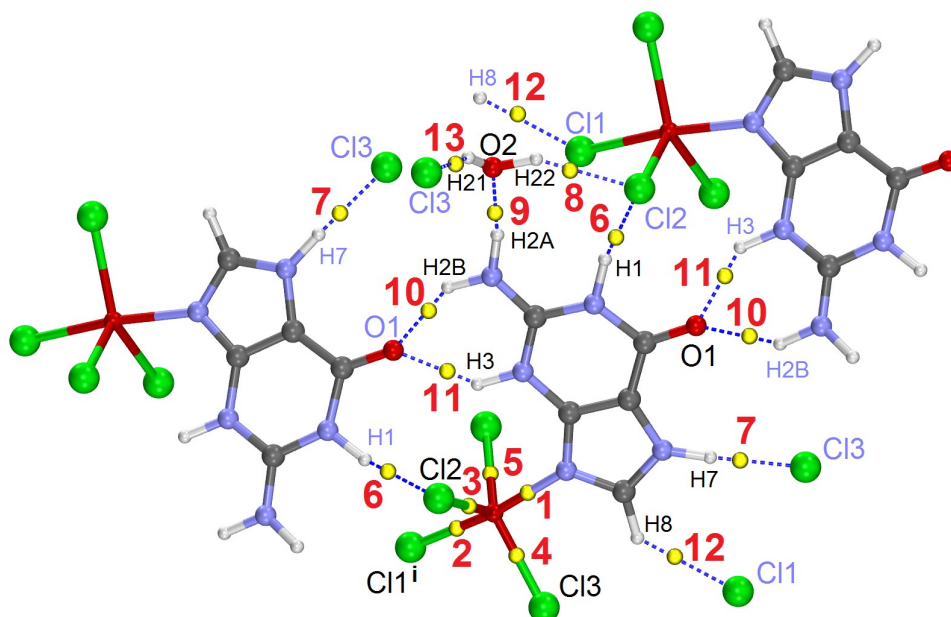
Fig. 6. The selected bond path (3, -1) critical points (BCP), yellow spheres marked with numbers in red colour, for intermolecular interactions in the (HGua)$_2$[Cu$_2$Cl$_6$]·2H$_2$O crystal. The QTAIM properties for BCPs 1-13 are in Table 4.

Conclusion

Crystals of $(HGua)_2[Cu_2Cl_6]\cdot 2H_2O$ (HGua = protonated guanine) were prepared and analysed by spectroscopic (IR, Raman) and computational methods. A new single-crystal X-ray diffraction analysis was conducted to obtain data with lower standard uncertainties than those in the previously published structure. Raman and IR spectroscopy and quantum-mechanical analysis have given us new insight into the vibrational states of the $(HGua)_2[Cu_2Cl_6]\cdot 2H_2O$ crystal. The vibrational spectra of the crystal were assigned by performing a normal coordinate analysis for a free dimer $(HGua)_2[Cu_2Cl_6]\cdot 2H_2O$ with a centre of inversion as the only symmetry element. The stretching vibration observed at 279 cm^{-1} in the infrared spectrum corresponds to the N−Cu bond. The NCI plots and QTAIM analysis of the electron density obtained from periodic DFT calculations gave us insight into the character, strength and direction of the interactions that exist within the crystal structure. The closed-shell ionic attractions and weak and medium strength hydrogen bonds prevail as interactions in the crystal structure. These new insights into the $(HGua)_2[Cu_2Cl_6]\cdot 2H_2O$ crystal structure can be used as an alternative model system of the DNA molecule, in which for the first time the DNA base environment contains two different ions, copper and chlorine, alongside the water molecule. As such, it might provide an important contribution to the study of charge transfer behaviour in the DNA model system, which could in turn contribute to the wider understanding of the possible mechanisms and possible paths by which the long-range charge transfer takes place.

Acknowledgments

References

[1] A. Fanget, F. Traversi, S. Khlybov, P. Granjon, A. Magrez, L. Forró, A. Radenovic, Nanopore integrated nanogaps for DNA detection, Nano Lett. 14 (2014) 244.
doi: 10.1021/nl403849g

[2] G.I. Livshits, A. Stern, D. Rotem, N. Borovok, G. Eidelshtein, A. Migliore, E. Penzo, S. J. Wind, R. Di Felice, S.S. Skourtis, J.C. Cuevas, L. Gurevich, A.B. Kotlyar, D. Porath, Long-range charge transport in single G-quadruplex DNA molecules, Nature Nanotechnology 9 (2014) 1040. doi: 10.1038/nnano.2014.246

[3] D. Porath, G. Cuniberti, R. Di Felice, Charge transport in DNA-based devices, Top. Curr. Chem. 237 (2004) 183. doi: 10.1007/b94477

[4] Z. Kabiljo, K. Sanković, J.N. Herak, ESR study of the thymine anion radical in a single crystal of thymine monohydrate, Int. J. Radiat. Biol. 58 (1990) 439.
doi: 10.1080/09553009014551791

[5] J.N. Herak, K. Sanković, J. Hüttermann, Thiocytosine as a radiation energy trap in a single crystal of cytosine hydrochloride, Int. J. Radiat. Biol. 66 (1994) 3.
doi: 10.1080/09553009414550891

[6] K. Sanković, D. Krilov, T. Pranjić-Petrović, J. Hüttermann, J.N. Herak, Nature of the chlorine-centred paramagnetic species in irradiated crystals of cytosine hydrochloride doped with thiocytosine, Int. J. Radiat. Biol. 70 (1996) 603. doi: 10.1080/095530096144815

[7] J.N. Herak, K. Sanković, D. Krilov, M. Jakšić, J. Hüttermann, Radiation energy-transfer and trapping in single-crystals of hemihydrate and hydrochloride of 5-methylcytosine doped with 5-methylthiocytosine - an EPR study, Radiat. Phys. Chem. 50 (1997) 141.
doi: 10.1016/s0969-806x(97)00027-3

[8] J.N. Herak, K. Sanković, D. Krilov, J. Hüttermann, An EPR study of the transfer and trapping of holes produced by radiation in guanine(thioguanine) hydrochloride single crystals, Radiation Research 151 (1999) 319. doi: 10.2307/3579944

[9] J.N. Herak, K. Sanković, E.O. Hole, E. Sagstuen, ENDOR study of a thiocytosine oxidation product in cytosine monohydrate crystals doped with 2-thiocytosine, X-irradiated at 15 K, Physical Chemistry Chemical Physics 2 (2000) 4971. doi: 10.1039/b004639f

[10] J.N. Herak, K. Sanković, E.O. Hole, E. Sagstuen, ENDOR study of the chlorinated thiocytosine radical in a crystal matrix, Physical Chemistry Chemical Physics 3 (2001) 4926.
doi: 10.1039/b106483p

[11] K. Sanković, E. Malinen, Z. Medunić, E. Sagstuen, J.N. Herak, Hole transfer in crystals of cytosine monohydrate: An EPR study, Physical Chemistry Chemical Physics 5 (2003) 1665. doi: 10.1039/b211108j

[12] G.A. Jeffrey, Y. Kinoshita, The crystal structure of cytosine monohydrate, Acta Cryst. 16 (1963) 20. doi: 10.1107/S0365110X63000049

[13] R.J. McClure, B.M. Craven, New investigations of cytosine and its monohydrate, Acta Cryst. B29 (1973) 1234. doi: 10.1107/S0567740873004292

[14] N.S. Mandel, The crystal structure of cytosine hydrochloride, Acta Cryst. B33 (1977) 1079. doi: 10.1107/S056774087700541X

[15] N. Padmaja, S. Ramakumar, M.A. Viswamitra, Structure of 5-methylcytosine hydrochloride, Acta Cryst. C43 (1987) 2157. doi: 10.1107/S0108270187088644

[16] C.T. Grainer, D. Bailey, The structure of the hemihydrate of 5-methylcytosine, a nucleic acid base, Acta Cryst. B37 (1981) 1561. doi: 10.1107/S0567740881006572

[17] C.E. Bugg, U. Thewalt, The crystal and molecular structure of 6-thioguanine, J. Am. Chem. Soc. 92 (1970) 7441. doi: 10.1021/ja00728a031

[18] J. Iball, H.R. Wilson, The Crystal and Molecular Structure of Guanine Hydrochloride Dihydrate, Proc. Roy. Soc. A288 (1965) 418. doi: 10.1098/rspa.1965.0232

[19] D. Matković-Čalogović, K. Sanković, Guaninium dichloride, Acta Cryst. C55 (1999) 467. doi: 10.1107/S0108270198014607

[20] D. Matković-Čalogović, E. Bešić, K. Sanković, 5-Methyl-2-thiouracil, Acta Cryst. C58 (2002) 568. doi: 10.1107/s010827010201315x

[21] B. Prugovečki, D. Matković-Čalogović, K. Sanković, 2-Thiocytosinium chloride, Acta Cryst. E61 (2005) 2706. doi: 10.1107/S1600536805023445

[22] K. Sanković, B. Prugovečki, D. Matković-Čalogović, 2-Thiocytosinium bromide, Acta Cryst. E61 (2005) 3846., doi: 10.1107/S1600536805033659

[23] J.P. Declercq, M. Debbaudt, M. Van Meerssche, Confirmation de la Structure Cristalline et Moléculaire du Complexe Guanine. $CuCl_2.Hcl.H_2O$, Bull. Soc. Chim. Belges 80 (1971) 527. doi: 10.1002/bscb.19710800522

[24] M. Sundralingam, J.A. Carrabine, Stereochemistry of nucleic acids and their constituents. XIX. Copper binding sites and mechanism of G-C selective denaturation of DNA. Crystal and molecular structures of guanine-copper(II) chloride and cytosine-copper(II) chloride complexes, J. Mol. Biol. 61 (1971) 287. doi: 10.1016/0022-2836(71)90381-0

[25] E.R. Johnson, S. Keinan, P. Mori-Sanchez, J. Contreras-Garcia, A.J. Cohen, W. Yang, Revealing noncovalent interactions, J. Am. Chem. Soc., 132 (2010) 6498.
doi: 10.1021/ja100936w.

[26] A. Otero-de-la-Roza, E.R. Johnson, J. Contreras-García, Revealing non-covalent interactions in solids: NCI plots revisited, Physical Chemistry Chemical Physics, 14 (2012) 12165. doi: 10.1039/C2CP41395G.

[27] G. Saleh, C. Gatti, L. Lo Presti, J. Contreras-García, Revealing Non☐covalent Interactions in Molecular Crystals through Their Experimental Electron Densities, Chemistry - A European Journal, 18 (2012) 15523. doi: 10.1002/chem.201201290.

[28] R.F.W. Bader, Atoms in Molecules: A Quantum Theory, Oxford University Press, Oxford, UK, 1990.

[29] P.L.A. Popelier, Atoms in Molecules: An Introduction, Pearson Education, Prentice Hall, 2000.

[30] CrysAlisPro, Agilent Technologies, Version 1.171.37.33 (release 27-03-2014)

[31] L.J. Farrugia, *WinGX* suite for small-molecule single-crystal crystallography, J. Appl. Cryst. 32 (1999) 837., doi: 10.1107/S0021889899006020

[32] G.M. Sheldrick, Acta Cryst. A short history of *SHELX*, A64 (2008) 112.
doi: 10.1107/S0108767307043930

[33] A.L. Spek, Single-crystal structure validation with the program PLATON, J. Appl. Cryst. 36 (2003) 7. doi: 10.1107/S0021889802022112

[34] C.F. Macrae, I.J. Bruno, J.A. Chisholm, P.R. Edgington, P. McCabe, E. Pidcock, L. Rodriguez-Monge, R. Taylor, M. Towler, J. Van der Streek, P.A. Wood, Mercury CSD 2.0 - New Features for the Visualization and Investigation of Crystal Structures, J. Appl. Cryst. 41 (2008) 466. doi: 10.1107/S0021889807067908]

[35] Gaussian 03, Revision E.01, M.J. Frisch, G.W. Trucks, H.B. Schlegel, G.E. Scuseria, M.A. Robb, J.R. Cheeseman, J.A. Montgomery, Jr., T. Vreven, K.N. Kudin, J.C. Burant, J.M. Millam, S.S. Iyengar, J. Tomasi, V. Barone, B. Mennucci, M. Cossi, G. Scalmani, N. Rega, G.A. Petersson, H. Nakatsuji, M. Hada, M. Ehara, K. Toyota, R. Fukuda, J. Hasegawa, M. Ishida, T. Nakajima, Y. Honda, O. Kitao, H. Nakai, M. Klene, X. Li, J.E. Knox, H.P. Hratchian, J.B. Cross, V. Bakken, C. Adamo, J. Jaramillo, R. Gomperts, R.E. Stratmann, O. Yazyev, A.J. Austin, R. Cammi, C. Pomelli, J.W. Ochterski, P.Y. Ayala, K. Morokuma, G.A. Voth, P. Salvador, J.J. Dannenberg, V.G. Zakrzewski, S. Dapprich, A.D. Daniels, M.C. Strain, O. Farkas, D.K. Malick, A.D. Rabuck, K. Raghavachari, J.B. Foresman, J.V. Ortiz, Q. Cui, A.G. Baboul, S. Clifford, J. Cioslowski, B.B. Stefanov, G. Liu, A. Liashenko, P. Piskorz, I. Komaromi, R.L. Martin, D.J. Fox, T. Keith, M.A. Al-Laham, C.Y. Peng, A. Nanayakkara,

M. Challacombe, P.M.W. Gill, B. Johnson, W. Chen, M.W. Wong, C. Gonzalez, J.A. Pople, Gaussian, Inc., Wallingford CT (2004)

[36] J.P. Perdew, Density-functional approximation for the correlation energy of the inhomogeneous electron gas, Phys. Rev. B33 (1986) 8822. doi: 10.1103/PhysRevB.33.8822

[37] J.P. Perdew, K. Burke, Y. Wang, Generalized gradient approximation for the exchange-correlation hole of a many-electron system, Phys. Rev. B54 (1996) 16533.
doi: 10.1103/PhysRevB.54.16533

[38] Y. Seki, A. Okazawa, M. Enomoto, J. Harada, K. Ogawa, N. Kojima, Alternating Ferro- and Antiferromagnetic Couplings in One-Dimensional Chain Hexachlorodicuprate(II), (MV)[$CuCl_3$]$_2$(MV = Methyl Viologen), Current Inorganic Chemistry 3 (2013) 94.
doi: 10.2174/1877944111303020004

[39] G. Perren, J.S. Mőller, D. Hűvonen, A.A. Podlesnyak, A. Zheludev, Spin dynamics in pressure-induced magnetically ordered phases in($C_4H_{12}N_2$)Cu_2Cl_6, Phys. Rev. B 92 (2015) 054413. doi: 10.1103/PhysRevB.92.054413

[40] CP2K version 2.6.2. The CP2K developers group, https://www.cp2k.org/, 2004.

[41] J. VandeVondele, M. Krack, F. Mohamed, M. Parrinello, T. Chassaing, J. Hutter, Quickstep: Fast and accurate density functional calculations using a mixed Gaussian and plane waves approach, Computer Physics Communications. 167 (2005) 103.
doi: 10.1016/j.cpc.2004.12.014.

[42] J.P. Perdew, K. Burke, M. Ernzerhof, Generalized Gradient Approximation Made Simple, Phys. Rev. Lett. 77 (1996) 3865. doi: 10.1103/PhysRevLett.77.3865.

[43] J.P. Perdew, A. Ruzsinszky, G.I. Csonka, O.A. Vydrov, G.E. Scuseria, L.A. Constantin, et al., Restoring the Density-Gradient Expansion for Exchange in Solids and Surfaces, Phys. Rev. Lett. 100 (2008) 136406. doi: 10.1103/PhysRevLett.100.136406.

[44] S. Goedecker, M. Teter, J. Hutter, Separable dual-space Gaussian pseudopotentials, Phys. Rev. B. 54 (1996) 1703. doi: 10.1103/PhysRevB.54.1703.

[45] C. Hartwigsen, S. Goedecker, J. Hutter, Relativistic separable dual-space Gaussian pseudopotentials from H to Rn, Phys. Rev. B. 58 (1998) 3641.
doi: 10.1103/PhysRevB.58.3641.

[46] J. VandeVondele, J. Hutter, Gaussian basis sets for accurate calculations on molecular systems in gas and condensed phases, The Journal of Chemical Physics. 127 (2007) 114105. doi: 10.1063/1.2770708.

[47] S. Grimme, J. Antony, S. Ehrlich, H. Krieg, A consistent and accurate *ab initio* parametrization of density functional dispersion correction (DFT-D) for the 94 elements H-Pu, The Journal of Chemical Physics. 132 (2010) 154104. doi: 10.1063/1.3382344.

[48] A. Otero-De-La-Roza, E.R. Johnson, V. Luaña, CRITIC2: A program for real-space analysis of quantum chemical interactions in solids, Computer Physics Communications. 185 (2014) 1007. doi: 10.1016/j.cpc.2013.10.026

[49] W. Humphrey, A. Dalke, K. Schulten, VMD: visual molecular dynamics, J. Mol. Graph. 14 (1996) 33., version 1.9.2. doi: 10.1016/0263-7855(96)00018-5.

[50] U. Thiewalt, C.E. Bugg, R.E. Marsh, The crystal structure of guanine monohydrate, Acta Cryst. B27 (1971) 2358. doi: 10.1107/S0567740871005880

[51] I. Turel, M. Pečanac, A. Golobič, E. Alessio, B. Serli, A. Bergamo, G. Sava, Solution, solid state and biological characterization of ruthenium(III)-DMSO complexes with purine base derivatives, J. Inorg. Biochem., 98 (2004) 393. doi: 10.1016/j.jinorgbio.2003.12.001

[52] A.S. Gaballa, H. Schmidt, C. Wagner, D. Steinborn, Structure and characterization of platinum(II) and platinum(IV) complexes with protonated nucleobase ligands, Inorg. Chim. Acta, 361 (2008) 2070. doi: 10.1016/j.ica.2007.10.023

[53] J.T. Blanchette, R.D. Willet, Magnetic and Structural Correlations in [(C_5H_5N)NH_2]$_2$$Cu_2Cl_6$ and [(C_5H_5N)NH_2]$_2$$Cu_2Br_6$·$H_2O$, Inorg.Chem. 27 (1988) 843.

doi: 10.1021/ic00278a019

[54] N.E. Kuz'mina, K.K. Palkina, N.V. Polyakova, I.N. Golubev, A.N. Medvedev, O.V. Koval'chukova, S.B. Strashnova, N.I. Mordovina, S.V.Nikitin, B.E. Zaitsev, Synthesis, structure, and magnetic properties of a copper(II) chloride complex with 3-amino-2-methyl-4H-pyrido[1,2-a]pyrimidin-4-one: The crystal structure $Cu(2)Cl(6)(C(9)H(10)N(3)O)(2)$ center dot $(C(9)H(10)N(3)O)Cl$, Russ. J. Inorg. Chem. 48 (2003) 205. doi:

10.1016/S0277-5387(00)84985-2

[55] M.A. Kurawa, C.J. Adams, A.G. Orpen, 2-Oxo-1,2- dihydropyrimidin-3-ium di-μ-chlorido-bis- {dichloridobis[pyrimidin-2(1H)-one- κN3]cuprate(II)} dehydrate, Acta Cryst. E64 (2008) 924. doi: 10.1107/S1600536808017455

[56] J M. Delabar, R. Majoube, Infrared and Raman spectroscopic study of 15N and D-substituted guanines, Spectrochimica Acta A34 (1978) 129. doi: 10.1016/0584-8539(78)80106-8

[57] M. Majoube, Ph. Millié, P. Lagant, G. Vergoten, Resonance Raman enhancement for adenine and guanine residues, J. Raman Spectrosc., 25 (1994) 821. doi: 10.1002/jrs.1250251008

[58] B. Giese, D. McNaughton, Density functional theoretical (DFT) and surface-enhanced Raman spectroscopic study of guanine and its alkylated derivatives Part 1. DFT calculations on neutral, protonated and deprotonated guanine, Phys. Chem. Chem. Phys. 4 (2002) 5161. doi: 10.1039/B203829C

[59] S. H. Rhim, Rolando Saniz, M. Weinert, A.J. Freeman, Superconductivity in CuCl/Si: possible excitonic pairing?, cond-mat. supr-con. (2015) arXiv:1510.03948

[60] E. Espinosa, I. Alkorta, J. Elguero, E. Molins, From weak to strong interactions: A comprehensive analysis of the topological and energetic properties of the electron density distribution involving X–H··· F–Y systems, J. Chem. Phys. 117 (2002) 5529. doi: 10.1063/1.1501133.

[61] R. Bianchi, G. Gervasio, D. Marabello, Experimental Electron Density Analysis of $Mn_2(CO)_{10}$: Metal−Metal and Metal−Ligand Bond Characterization, Inorganic Chemistry 39 (2000) 2360. doi: 10.1021/ic991316e.

[62] S. Janusz Grabowski, What Is the Covalency of Hydrogen Bonding?, Chem. Rev. 111 (2011) 2597. doi: 10.1021/cr800346f.

SUPPLEMENTARY DATA

New Investigations of the Guanine Trichloro Cuprate (II) Complex: (HGua)$_2$[Cu$_2$Cl$_6$]·2H$_2$O

Ivana Fabijanić, Dubravka Matković-Čalogović, Viktor Pilepić, Irena Ivanišević, Vlasta Mohaček-Grošev, and Krešimir Sanković

Raman and IR spectra

Fig. S1. IR and Raman spectra of the crystalline (HGua)$_2$[Cu$_2$Cl$_6$]·2H$_2$O.
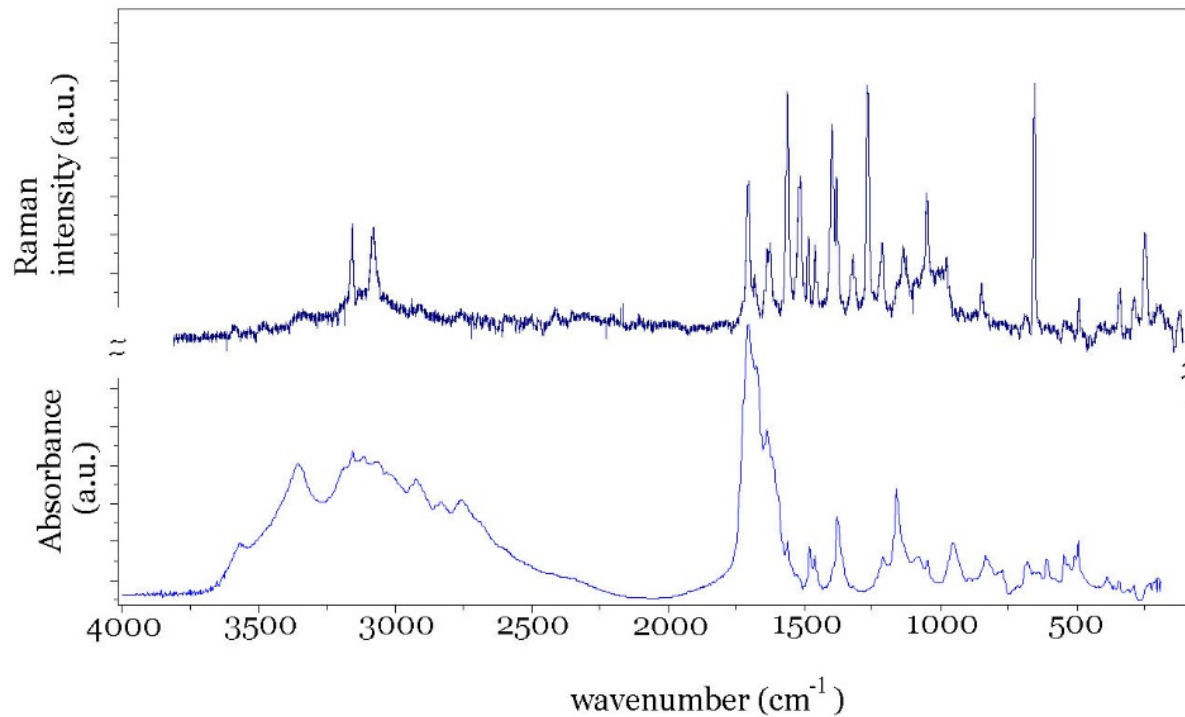
Table S1. Observed Raman and infrared bands of the polycrystalline $(HGua)_2[Cu_2Cl_6]\cdot 2H_2O$ crystal are compared with the calculated values for normal mode vibrations of a dimer obtained with B3PW91 functional and 3-21G basis set using the Gaussian03 program. The bands' positions are given in cm^{-1}. A_g is in-phase symmetrical dimer vibration, and A_u is out-of-phase antisymmetrical dimer vibration, ν – stretching, δ – bending, Φ – in plane bending, μ – out of plane bending, br – broad, vbr – very broad, w – weak, sh – shoulder.

Observed		Calculated		
Raman	Infrared	A_g Raman	A_u infrared	mode description
		3672		$\nu_{asym}(NH_2)$
	3564		3672	$\nu_{asym}(NH_2)$
		3608		$\nu(N7–H7)$
	3352		3607	$\nu(N7–H7)$
		3555		$\nu(N1–H1)+\nu_{sym}(NH_2)$
	3184		3555	$\nu(N1–H1)+\nu_{sym}(NH_2)$
	3155		3545	$\nu(N1–H1)+\nu_{sym}(NH_2)$
3157		3545		$\nu(N1–H1)+\nu_{sym}(NH_2)$
	3113		3519	$\nu_{asym}(H_2O)$
3108 vbr		3518		$\nu_{asym}(H_2O)$
3078 br		3412		$\nu_{sym}(H_2O)$
	3065		3412	$\nu_{sym}(H_2O)$
3059		2693		$\nu_{sym}(C8–H8)$
		3016		
	2939		2693	$\nu_{asym}(C8–H8)$
	2922			
	2905			
	2831			
	2756			
			2516	$\nu_{asym}(N3–H3)$
	2686	2511		$\nu_{sym}(N3–H3)$
1704		1824		$\nu(C6=O1)$
	1703		1822	$\nu(C6=O1)$
		1717		$\delta(NH_2)$ scissoring
	1688		1716	$\delta(NH_2)$ scissoring
		1708		$\delta(H3–N3–C2)$
	1674		1705	$\delta(H3–N3–C2)$
1635		1672		$\delta(H_2O)$
	1635		1672	$\delta(H_2O)$
	1616		1651	$\nu(C4=C5)$
1624		1651		$\nu(C4=C5)$
1596		1602		$\nu(N9–C4)$
	1593		1601	$\nu(N9–C4)$
1560		1569		$\nu(C2–N3)$
	1562		1569	$\nu(C2–N3)$
1515				
1484		1489		$\Phi(C8–H8)$ in plane bend.
	1477		1488	$\Phi(C8–H8)$ in plane bend.
1458		1481		$\Phi(N7–H7)$

Table S1 continued

| Observed | | Calculated | | |
Raman	Infrared	A_g Raman	A_u infrared	Mode description
	1458		1481	Φ(N7–H7)
1397		1415		Φ(N1–H1)
	1394		1415	Φ(N7–H7)
	1377		1386	Φ(C8–H8)+ν(C5–C6)
1379		1384		Φ(C8–H8)+ν(C5–C6)
		1373		ν(C5–N7)
			1372	ν(C5–N7)
	1319		1323	ν(N7–C8)
1320		1322		Φ(C8–H8)+ ν(C8–N9)
1266		1281		Φ(C8–H8)+ ν(C8–N9)
			1281	ν(C8–N9)
1240		1234		ν(C8–N9)+ ν(C5–N7)
	1234		1233	ν(C8–N9)+ ν(C5–N7)
1213	1211	1154		ν(N7–C8)
1154	1159		1153	ν(N7–C8)
	1133		1125	δ(NH$_2$)
1135		1124		δ(NH$_2$)
		1069		ν(C2–N3)+ ν(N1–C2)
	1080 br		1069	ν(C2–N3)+ ν(N1–C2)
	1047		1041	two rings stretching
1049		1041		two rings stretching
			1012	μ (N3–H3)
1031		1012		μ (N3–H3)
1009		1010		pyrimidine ring breathing
994				
978				
	951 br		1007	pyrimidine ring breathing
	895 w		912	μ(N3–H3)+ μ(C6–O1)
		912		μ(N3–H3)+ μ(C6–O1)
850		881		δ(N2–C2–N3)
	833		879	δ(N2–C2–N3)
	812 sh		810	Φ(N1–H1)
		809		Φ(N1–H1)
		767		out of plane guanine deformation
	779 br		767	out of plane guanine deformation
		749		Φ(N7–H7)
	729 w		749	Φ(N7–H7)
		710		μ(N7–H7)+μ(N1–H1)
	717 w		709	μ(N7–H7)+μ(N1–H1)
687		675		In plane NH$_2$ bending
	683		675	In plane NH$_2$ bending
656		659		μ(NH$_2$) asym.
	658		659	μ(NH$_2$) asym.

Table S1 continued

| Observed | | Calculated | | |
Raman	Infrared	A_g Raman	A_u infrared	mode description
		647		δ(N9–C4–N3)
	640		646	μ(NH$_2$) sym.
	609		629	μ(NH$_2$) sym.
		629		H$_2$O wagging
608		609		H$_2$O wagging
			599	H$_2$O twisting
581 w		573		H$_2$O twisting
			571	in plane ring bending
541		551		δ(C4–N3–C2)
	546		551	δ(C4–N3–C2)
	530			
	507		505	Pyrimidine ring in pl. def.
		504		Pyrimidine ring in pl. def.
492	496			
471		439		H$_2$O libration
			437	H$_2$O libration
417		419		ring twisting
			418	ring twisting
397		381		NH$_2$ torsion
	390			
	380		381	NH$_2$ torsion
	364		365	δ(Cu–N9–C8)+ δ(N7–C5–C6)
368		364		δ(Cu–N9–C8)+ δ(N7–C5–C6)
344		344		NH$_2$ in plane bending
	347		343	NH$_2$ in plane bending
		329		Cu–N9 out of plane deformation
			323	Cu–N9 out of plane deformation
313		320		ring flapping around C4=C5
	312		319	ring flapping around C4=C5
	293		297	C5=C6 out of plane def.
290		293		ν(Cu–N9)+Cl1, Cl1^i translation
		279		ν(Cu–N9)+Cl1, Cl1^i translation
			261	δ(O1–C6–C5)+imidazole def.
250		249		H$_2$O translation
			244	H$_2$O translation
		225		chlorine translation + ring def.
			219	chlorine translation + pyrimid. ring def.
		209		chlorine translation + pyrimid. ring def.
			206	pyrimidine torsion
		204		pyrimidine torsion
195		197		δ(Cu–N9–C4)
			185	chlorine translation
			170	Imidazole-pyrimidine bend
			160	guanine out of plane def.
166		160		guanine out of plane def.

Table S1 continued

Observed		Calculated		
Raman	Infrared	A_g Raman	A_u infrared	mode description
154		155		Cl2, Cl2^i translation
		139		guanine out of plane def.
			135	chlorine translation
			135	guanine out of plane def.
			128	guanine out of plane def.
		125		H_2O translation
		109		H_2O translation
			107	ν(Cu–Cl2)+H_2O transl.
		105		ν(Cu–Cl2)+H_2O transl.
			97	δ(Cu–N9–C8)+Cl transl.
		96		δ(Cu–N9–C8)+Cl transl.
			84	chlorine + H_2O translation
		83		chlorine + H_2O translation
			82	Cl2, Cl2^i + H_2O translation
		73		Cl2,Cl2^i + H_2O translation
		62		Cl3,Cl3^i + H_2O translation
			56	Cl3,Cl3^i + H_2O translation
		44		guanine libration
			34	guanine libration
			22	guanine libration
		17		N9–Cu–Cu^i bending
			11	guanine libration

Fig. S2. Non-covalent interaction (NCI) domains in the $(HGua)_2[Cu_2Cl_6]\cdot 2H_2O$ crystal cell. The reduced gradient isosurfaces at $s = 0.35$ a.u. are given on a red-green-blue colour scale according to the sign $(\lambda_2)\rho$ values ranging from -0.05 to 0.05 a.u. indicating the repulsive non-bonding, weak attractive and strong attractive interactions, respectively.